Pyruvate prevents the development of age-dependent cognitive deficits in a mouse model of Alzheimer's disease without reducing amyloid and tau pathology

Elisa Isopi[a], Alberto Granzotto[a], Carlo Corona[a], Manuela Bomba[a], Domenico Ciavardelli[a,b], Michele Curcio[c], Lorella M.T. Canzoniero[c], Riccardo Navarra[d], Rossano Lattanzio[e], Mauro Piantelli[e], and Stefano L. Sensi[a,d,f]

Affiliations

[a] Molecular Neurology Unit, Center of Excellence on Aging (Ce.S.I.), "G. d'Annunzio" University, Chieti, 66100, Italy

[b] School of Human and Social Science, "Kore" University of Enna, Enna, 94100, Italy

[c] Department of Biological and Environmental Science, University of Sannio, Benevento, 82100, Italy

[d] Department of Neuroscience and Imaging, "G. d'Annunzio" University, Chieti, 66100, Italy

[e] Department of Clinical and Experimental Sciences, "G. d'Annunzio" University, Chieti, 66100, Italy

[f] Departments of Neurology and Pharmacology, Institute for Memory Impairments and Neurological Disorders, University of California-Irvine, Irvine, 92697, California, United States of America

Correspondence should be addressed: Stefano L. Sensi, Molecular Neurology Unit, Center of Excellence on Aging (Ce.S.I.), "G. d'Annunzio" University, Via Luigi Polacchi 11, 66100, Chieti, Italy.
E-mail: ssensi@uci.edu.
Phone number: 0871 541544

Abstract

Amyloid-β (Aβ) deposition and tau-dependent pathology are key features of Alzheimer's disease (AD). However, to date, approaches aimed at counteracting these two pathogenic factors have produced only modest therapeutic outcomes. More effective therapies should therefore consider additional pathogenic factors like energy production failure, hyperexcitability and excitotoxicity, oxidative stress, deregulation of metal ion homeostasis, and neuroinflammation.

Pyruvate is an energy substrate associated with neuroprotective properties. In this study, we evaluated protective effects of long-term administration of pyruvate in 3xTg-AD mice, a preclinical AD model that develops amyloid-β- and tau-dependent pathology.

Chronic (9 months) treatment with pyruvate inhibited short and long-term memory deficits in 6 and 12 months old 3xTg-AD mice as assessed with the Morris water maze test. Pyruvate had no effects on intraneuronal amyloid-β accumulation and, surprisingly, the molecule increased deposition of phosphorylated tau. Pyruvate did not change aerobic or anaerobic metabolisms but decreased lipid peroxidation, counteracted neuronal hyperexcitability, decreased baseline levels of oxidative stress, and also reduced reactive oxygen species-driven elevations of intraneuronal Zn^{2+} as well as glutamate receptor-mediated deregulation of intraneuronal Ca^{2+}.

Thus, pyruvate promotes beneficial cognitive effects without affecting Aβ and tau pathology. The molecule mainly promotes a reduction of hyperexcitability, oxidative stress while favors the regulation of intraneuronal Ca^{2+} and Zn^{2+} homeostasis rather than acting as energy substrate.

Pyruvate can be therefore a valuable, safe, and affordable pharmacological tool to be associated with classical anti-Aβ and tau drugs to counteract the development and progression of AD-related cognitive deficits and neuronal loss.

Keywords: Pyruvate, Alzheimer's disease, 3xTg-AD mice, oxidative stress, brain metabolism, amyloid, tau, zinc

Abbreviations: Alzheimer's disease (AD), amyloid-β (Aβ), neurofibrillary tangles (NFTs), hyperphosphorylated tau (p-tau), reactive oxygen species (ROS), intraneuronal Zn^{2+} $[Zn^{2+}]_i$, intraneuronal Ca^{2+} $[Ca^{2+}]_i$, month old (m.o.), months of age (m.o.a.), intraperitoneal injection (i.p.), Morris water maze (MWM), complex I, II, IV, and V (CI, CII, CIV and CV), lactate dehydrogenase (LDH), 2,2'-dithiodipyridine (DTDP), N-Methyl-D-aspartate (NMDA), blue-native polyacrylamide gel electrophoresis (BN-PAGE), gas chromatography coupled to mass spectrometry (GC-MS), thiobarbituric reactive substances (TBARS), N-methyl-D-aspartate receptor (NMDAR), Hydroethidine (HEt).

Introduction

Amyloid-β (Aβ) oligomers and the deposition of amyloid plaques, along with the formation of neurofibrillary tangles (NFTs) made of hyperphosphorylated tau (p-tau), are considered key pathogenic determinants of Alzheimer's disease (AD; Hardy and Higgins, 1992; Hardy and Selkoe, 2002). However, to date, therapeutic approaches aimed at counteracting Aβ dysmetabolism and tau-related pathology have only produced very modest therapeutic results. A more comprehensive line of intervention aimed at effectively addressing additional and complementary pathogenic factors is therefore greatly needed.

AD is a clinically heterogeneous and multi-factorial disorder. On the permissible background offered by the aging brain, energy production failure, mitochondrial dysfunction, neuronal hyperexcitability, excitotoxicity, oxidative stress, alteration of brain levels of metal ions (Ca^{2+}, Zn^{2+}, Cu^{2+}, Fe^{3+}), neuroinflammation, deregulation of neurotrophic factors, all synergistically act to promote AD-related pathology and cognitive decline (Ittner and Götz, 2011).

Hippocampal hyperactivation, a phenomenon found in preclinical AD models and patients (Bakker et al., 2012; Vossel et al., 2013) leads to network instability, cognitive dysfunction and can trigger an excitotoxic overdrive that is instrumental to promote the neuronal loss found in the disease (Palop and Mucke, 2009). Excitotoxicity is central for the injurious deregulation of intraneuronal Ca^{2+} ($[Ca^{2+}]_i$) and Zn^{2+} ($[Zn^{2+}]_i$) (Sensi et al., 2009). Deregulation of brain Zn^{2+} homeostasis, in particular, exacerbates Aβ oligomerization, NFT formation, mitochondrial dysfunction and also furthers the generation of oxidative stress (Sensi et al., 2009; Bush, 2013).

Pyruvate, the end product of glycolysis possesses antioxidant properties and protects against excitotoxic insults *in vitro* and *in vivo* (Maus et al., 1999; Gramsbergen et al., 2000; Izumi and Zorumski, 2010). Interestingly, pyruvate strongly attenuates neuronal death resulting from exposure to extracellular Zn^{2+} (Sheline et al., 2000) and is neuroprotective against the Zn^{2+}-dependent neuronal loss observed in animal models of transient cerebral and retinal ischemia (Lee et al., 2001; Yoo et al., 2004). As for AD, oxidative stress dependent Zn^{2+} deregulation has been found in cultured neurons obtained from the 3xTg-AD mouse, a widely employed preclinical AD model (Sensi et al., 2008). In cultured 3xTg-AD cortical neurons, ($[Zn^{2+}]_i$ rises triggered by oxidation were in fact found to be significantly increased compared to non-Tg cultures, thereby indicating the presence of a distinct intracellular milieu that is likely making the cells more susceptible to Zn^{2+}-dependent neuronal injury (Sensi et al., 2008).

In light of these observations, we explored whether chronic administration of pyruvate is beneficial in the 3xTg-AD model. The model seems particularly suitable for preclinical studies as this AD mouse develops both amyloid- and tau-dependent pathology along with oxidative stress, Ca^{2+} and Zn^{2+} deregulation, hyperexcitability and also shows an acceleration in the expression of genes that are actively associated with aging (Chakroborty et al., 2012; Gatta et al., 2014).

Materials and methods

Chemicals

FluoZin-3 AM, Fluo-4FF AM, Fluo-4 AM, Hydroethidine (Het) and pluronic acid were purchased from Molecular Probes (Life Technologies). Sodium pyruvate, N-Methyl-D-aspartate (NMDA), 2,2'-dithiodipyridine (DTDP), glycine as well as chemicals employed to prepare HEPES-buffered control salt solution (see below) and perform blue-native polyacrylamide gel electrophoresis (BN-PAGE), were purchased from Sigma-Aldrich. Cell cultures media and sera were purchased from Gibco (Life Technologies).

Animal model

All experiments employing animal models were approved by the local institutional Ethical Committee (CeSI protocol #: AD-301) and in compliance with national (D.L. n. 116, G.U., suppl. 40, 18 February 1992) and international laws and policies. 3xTg-AD mice were generously provided by Frank LaFerla. Mice were grouped-housed, given access to food and water *ad libitum* and maintained in a 12:12 light:dark cycle. Behavioral tests were performed during light phase of the cycle.

3 month old (m.o.) male and female 3xTg-AD mice were treated with an intraperitoneal injection (i.p.) of 500 mg/Kg pyruvate for a period of 9 months. The goal of the study was to evaluate effects of chronic pyruvate treatment and, given the plasmatic half-life of the molecule (Choi et al., 2013), we set to treat mice three times per week to achieve and maintain high pyruvate levels o in the brain. The 3xTg-AD control group was treated with a saline solution. 12 m.o. 3xTg-AD mice were killed and brains sampled as previously described (Corona et al., 2010).

Cell cultures

Near-pure neuronal cultures were prepared from embryonic (E15 or E16) 3xTg-AD mice. Cerebral cortices were removed and dissected in ice-cold dissecting medium and then placed in trypsin (0.25%) for 10 minutes at 37°C. Tissue was centrifuged, supernatant discarded, and pellet mechanically dissociated with a glass Pasteur pipette. Cells were then re-suspended in plating medium containing Neurobasal Medium supplemented with L-Glutamine (0.5 mM), 5% fetal bovine serum, 5% horse serum, 1 × B27, and 0.2% penicillin/streptomycin. Cell suspensions were plated onto 25 mm glass bottom dishes pretreated with poly-DL-lysine and laminin (Sigma-Aldrich) and incubated in a controlled atmosphere (5% CO_2 and 90% humidity). 3 days after plating, non-neuronal cell growth was inhibited by adding 10 µM of cytosine arabinofuranoside. Twice a week, 25% of the medium was replaced with equal amounts of fresh Neurobasal medium. Neurons were used after 12 to 17 days (D.I.V.) *in vitro.* The age-range of the cultures was chosen as full maturation of NMDA and AMPA receptors occurs by the 12 D.IV. (Jones and Baughman, 1991; Li et al., 1998; Stanika et al., 2009). We have previously and extensively employed neuronal cultures within this age bracket and found, in this and previous studies, comparable results in terms of NMDAR-evoked responses when investigating cation deregulation and subsequent mitochondrial dysfunction (Dugan et al., 1995; Sensi et al., 1997; Canzoniero et al., 2013). In agreement with our previous studies, no differences were found for these endpoints (cation deregulation and mitochondrial effects) in present neuronal cultures assayed at the two opposite sides of the 12-17 D.I.V. spectrum.

Morris water maze (MWM) test

MWM tests were performed according to what previously described (Masciopinto et al., 2012). Briefly, the same mice were tested at 6 and 12 m.o.a., howewer, upon statistical analysis, Grubb's test was performed to detect outliers and led us to evaluate, in the final statistical analysis, a slightly reduced number of mice per condition . Both 6 m.o. (treated, n=27; untreated n= 18) and 12 m.o. (treated, n=22; untreated, n=19) 3xTg-AD mice were trained for 3 consecutive days with four trials per day and an inter-trial time of 20 minutes. 1.5 and 24 hours after the end of the last training trial, probe tests were conducted to assess retention of the spatial memory. During both probe trials, the platform was removed from the pool (Panlab/Harvard apparatus) and mice were allowed to swim freely for 60 seconds. Parameters employed to evaluate memory skills were time spent to reach the platform location (latency) and number of crosses over the platform location

(crosses).

Immunohistochemistry

Immunohistochemistry analysis was carried out in accordance with a previously employed protocol (Corona et al., 2010). Mice to be assayed with immunohistochemistry analysis were randomly chosen from pool of mice that had been behaviorally tested before the assay. Briefly, carnoy-fixed and paraffin-embedded brains of treated (p-tau and Aβ, n=12) and untreated (p-tau, n=10; Aβ, n=11) 3xTg-AD mice were sagittally sectioned. Antigen retrieval was performed by microwave treatment at 750 W for 10 minutes for p-tau and by water bath at 100°C for 20 minutes for Aβ, both in 10 mmol/L sodium citrate buffer (pH 6.0). Tissue sections were incubated overnight with the primary antibody, after the secondary antibody incubation, counterstained with Mayer's hematoxylin, and reactions visualized using diamminobenzidine as chromogen. The anti-mouse EnVision kit (Dako) was used for signal amplification. Immunostaining signal evaluation was performed counting stained pixels on hippocampal cells by Photoshop version 8.0 (Adobe System Incorporated) as previously reported (Corona et al., 2010). The following antibodies were used: anti-Aβ clone DE2B4, diluted 1:400 (Abcam) and anti-p-tau clone AT180, diluted 1:400 (Pierce).

Mitochondrial sample preparation and BN-PAGE

Samples for BN-PAGE were prepared as previously described by Schägger (Schägger et al., 1996; Corona et al., 2010) with minor modifications. After solubilization of mitochondrial membranes by dodecyl maltoside, 20 mg of each sample were loaded on a 6-13% gradient acrylamide gel and subjected to electrophoresis on ice. For each gel set, one gel was stained with Coomassie blue and one was used to determine enzymatic activities. Complex I, II, IV (C I, C II and C IV) activities were assessed as previously described (Corona et al., 2010). Complex V (C V) activity was measured by incubating overnight gels in 35 mM Tris-HCl, 270 mM glycine, 14 mM $MgSO_4$, 0.2% $Pb(NO_3)_2$, and 8 mM ATP, pH 7.8, at room temperature; the reaction was stopped in 50% methanol and gels washed in distilled water before the acquisition of the images. Violet colored complex bands (and red-stained C IV bands) were captured using the Bio-Rad Imaging Densitometer (Quantity One Analysis Software, BioRad) with a blue filter inserted to minimize interference from the residual Coomassie Blue. The band area was expressed as absolute values

(in arbitrary units) and optical densities of bands of mitochondrial complex activities plotted against the respective value as determined in the Coomassie Blue gel.

NAD^+: NADH ratio determination

NAD^+: NADH ratio was determined in brain tissue homogenized as described below. The ratio was carried out using a EnzyChrome NAD^+: NADH Assay Kit (Gentaur) according to the manufacturer specifications.

Analysis of cytosolic lactate dehydrogenase (LDH) activities

LDH is composed by the two subunits, H and M, and present as five tetrameric isozymes. These isozymes catalyze the forward or backward conversion of pyruvate to lactate. The M subunit, encoded by the LDHA gene, promotes the conversion of pyruvate to lactate. In contrast, the H subunit, encoded by the LDHB gene, converts lactate to pyruvate that is further oxidized. Forward ($LDH_{Pyr\text{-}Lac}$) and reverse ($LDH_{Lac\text{-}Pyr}$) LDH activities were assayed spectrophotometrically as previously described (Bomba et al., 2013). Briefly, treated (n=3) and untreated (n=3) brain tissues were homogenized in phosphate buffer solution (20 mL/g of tissue, 0.010 M, pH=7.4). Homogenates were centrifuged at 2,000 g for 3 minutes at 4°C to remove cell debris and nuclear pellets. Supernatants were further centrifuged at 8,000 g for 10 minutes at 4°C to obtain cytosolic fractions. Protein concentration was determined according to Bradford assay. $LDH_{Pyr\text{-}Lac}$ activity determination was achieved by adding pyruvate (25 µL, 2.50 g/L) and reduced NADH (100 µL, 0.3 g/L) to the samples (50 µL). Decrease of absorbance at 340 nm was measured at 25°C in 1 minute intervals for 5 minutes. $LDH_{Lac\text{-}Pyr}$ activity determination was achieved by adding lactate (25 µL, 8.6 g/L) and NAD^+ (100 µL, 3.5 g/L) to the sample (25µL). Increase of absorbance at 340 nm was measured as described above. Forward and reverse LDH activities were expressed as µmol/($mg_{protein}$/min).

Determination of brain lactate by gas chromatography coupled to mass spectrometry (GC-MS)

Lactate levels were quantified in brain tissues collected from treated and untreated mice (n=3 per each group) by GC-MS. Briefly, cytosolic brain homogenates (50 µL) were treated as

previously described (Bomba et al., 2013) and GC-MS analysis performed using a 6890N gas-chromatograph equipped with a 7863 Series auto-sampler and coupled with a 5973N mass spectrometer (Agilent Technologies) operating in electron impact ionization mode. Injection was performed in pulsed-splitless mode by applying a pressure of 80 psi. Injector temperature was kept at 250 °C. Chromatographic separations were obtained using a fused silica capillary column HP-5MS (30m x 0.25 mm, Agilent Technologies). Helium was used as carrier gas at a constant flow rate of 1 mL min^{-1}. GC oven was programmed to start at 70 °C (holding time of 1 minute) and temperature raised at 4°C min^{-1} to reach 300 °C (holding time of 5 minutes). The mass spectrometer was automatically calibrated using per-fluoro tributylamine as calibration standard. For quantification, the mass spectrometer was used in selective ion monitoring mode and mass spectra recorded in positive modes by monitoring m/z 147 (lactic acid) and 251 (13C4 succinic acid, IS). Mass spectrometer parameters were: interface temperature 300 °C, ion source 250 °C, and quadrupole 150 °C. The external standard method and internal standard correction were applied for quantification. Data acquisition was performed with the G1701CA ChemStation software (Agilent Technologies).

Thiobarbituric reactive substances (TBARS) assay

Lipid peroxidation was assessed by TBARS assay. Brain tissues collected from treated (n=3) and untreated (n=2) 3xTg-AD mice were homogenized in an ice-cold cell extraction buffer (Life Technologies) supplemented with protease and phosphatase inhibitors (Life Technologies) and phenylmethanesulfonyl fluoride (Sigma-Aldrich). After 30 minutes of incubation on ice, homogenates were centrifuged at 3,000 g for 10 minutes at 4°C. Supernatants were diluted in 2 vol of 10% trichloroacetic acid and incubated for 15 minutes on ice. Samples were centrifuged at 2,200 g for 15 minutes and supernatants were added to an equal volume of 0.67% TBA and heated to 100°C for 10 minutes. After cooling, the formation of TBARS was spectrophotometrically determined by measuring the absorbance at 532 nm. The amount of TBARS in the samples was calculated from a standard curve produced by hydrolysis of tetraethoxypropane. Results were normalized to protein concentration.

Imaging studies

Intraneuronal Ca^{2+} and Zn^{2+} measurements

For Ca^{2+} and Zn^{2+} imaging experiments, neuronal cultures were washed three times in HEPES-buffered control salt solution (composition in mM: 120 NaCl, 5.4 KCl, 0.8 $MgCl_2$, 20 HEPES, 15 glucose, 1.8 $CaCl_2$, 10 NaOH; pH 7.4) as previously described (Sensi et al., 1999a). Cultures were loaded in the dark for 30 minutes at 25°C with the high affinity Ca^{2+} indicator Fluo-4 or the low affinity Ca^{2+} indicator Fluo-4FF (both at 3µM + 0.2% pluronic acid) or the Zn^{2+}-sensitive probe FluoZin-3 (5µM + 0.2% pluronic acid). Cultures were then washed in HEPES-buffered control salt solution for additional 30 minutes to allow probe de-esterification. Loading and de-esterification were conducted in the presence or absence of 10 mM pyruvate. Zn^{2+} imaging experiments were carried out on a Nikon Eclipse TE 300 microscope equipped with a Xenon lamp, a filter wheel (Lambda shutter 10-2, Sutter Instruments) and a 40x epifluorescence oil immersion objective (N.A.: 1.4; Nikon). Excitation and emission were set at 490 nm and 510 nm respectively, as previously described (Sensi et al., 1999a). Images were collected every 10 seconds using a 12-bit CCD camera (Orca, Hamamatsu) and analyzed with Metafluor 6.0 software (Molecular Devices). Ca^{2+} imaging experiments were carried out on an Axio Examiner.D1 upright microscope (Zeiss) equipped with a Xenon lamp-based Optoscan monochromator (Cairn), a 40x W Plan-Apochromat (N.A.: 1.0; Zeiss) and a 16-bit Evolve 512 EMCCD camera (Photometrics). Excitation and emission were set at 478 nm and 525 nm, respectively. Images were acquired every 20 seconds and stored for offline analysis by using Metamorph 7.7 software (Molecular Devices).

After background subtraction from a cell-free region of the dish, fluorescence variations were expressed as: $F=F_x/F_0$, where F_0 is fluorescence value at baseline and F_x is the fluorescence value obtained for each cell. Drugs were applied and removed through a rapid flow exchange system. Values are reported as mean ± SEM of F_x/F_0 ratio.

Spontaneous synaptic activity was assessed by high speed Ca^{2+} imaging in Fluo-4 AM loaded neurons sampled at 2 Hz (a sampling speed that, after pilot experiments in which a range of 10 to 1Hz acquisitions were tested, was found the best compromise to fully assess activity while avoiding probe bleaching). For each dish, three different regions of dispersed un-clustered neurons were chosen to measure spikes. Exposure time was set at 5 ms to avoid dye photobleaching and the signal was enhanced with an electromultiplier to achieve an optimal signal-to-noise ratio. Normalized $[Ca^{2+}]_i$ transients were analyzed as far as variations in frequency and amplitude values by employing a custom-made Matlab script.

Reactive oxygen species (ROS) generation measurements

For ROS measurements, cultures were loaded in the dark with HEt (5µM) for 45 minutes at 25°C and the same HEt concentration was maintained in the medium throughout each experiment (Sensi et al., 1999b). To minimize dye photo oxidation, images were collected at 2 minutes intervals. Cells were excited at 540 nm and emission monitored at > 590 nm. Baseline fluorescence intensities of pyruvate-treated neurons were normalized to values obtained in untreated sister cultures and expressed as percentage of these values. Background subtraction was performed from a cell-free region of the dish. Drugs were applied in a static bath.

Statistical analysis

Behavioral data were analyzed with Two-way factorial ANOVA followed by Fisher LSD post hoc test using the general linear model approach that considers an unequal sample size of the study groups. Aligned rank transformation of data was performed using ARTweb free software as previously described (Masciopinto et al., 2012). Outliers were detected using Grubb's test. Mann-Whitney Test was performed to assess statistical significance between immunohistochemical treated and untreated samples. Metabolic, TBARS and imaging data were evaluated for statistical significance using the two-tailed Student's t-test for unpaired comparisons between treated and untreated groups (95% confidence level). P values are represented as * ($p \leq 0.05$) or ** ($p \leq 0.01$).

Results

Pyruvate administration counteracts the development of age-dependent memory deficits in 3xTg-AD mice

As previously reported, 3xTg-AD mice start to develop memory deficits at 5-6 months of age (m.o.a., Billings et al., 2005). To evaluate whether chronic administration of pyruvate decreases cognitive impairment in our model, 3 m.o. 3xTg-AD mice were treated for a 9 month period with an i.p. injection of 500 mg/Kg of pyruvate. The rationale for the chosen dose comes from evidence indicating that at this concentration, given the first pass partial drug metabolization by the liver, there is still significant pyruvate permeation across the blood-brain barrier (Miller and Oldendorf, 1986), thereby allowing the building up of significant levels of pyruvate in the brain (Fukushima et al., 2009). Furthermore, 500 mg/Kg of pyruvate has been

successfully employed in previous studies aiming at promoting neuroprotection in rat models of epilepsy or diabetes (Suh SW et al., 2005; Kim et al., 2007).

6 and 12 m.o. 3xTg-AD mice were cognitively evaluated with the MWM test, a hippocampus-dependent task employed to investigate spatial memory (Sutherland and McDonald, 1990). At the end of the training period, mice were studied 1.5 and 24 hours after the last trial session to assess short- and long-term memory performances, respectively. Results of this set of experiments indicate that pyruvate treatment produced a significant improvement of short- and long-term memory performances in 6 m.o. 3xTg-AD mice as shown by the increased number of platform crosses (Fig. 1A, p=0.038; 1B, p=0.013). 12 m.o. treated-3xTg-AD mice also preserved cognitive performances as indicated by reduced latencies at 1.5 and 24 hours (Fig. 1C, p=0.034; 1D, p=0.017) and by the increased number of platform crosses in the short-term memory test (Fig. 1A, p=0.041). Analysis of long-term memory performances showed a trend toward beneficial effects that did not reach statistical significance (Fig. 1B, p=0.056).

Pyruvate does not affect intraneuronal Aβ deposition while exacerbates tau pathology in the hippocampus of 3xTg-AD mice

In search for mechanisms by which pyruvate supplementation may have acted to improve cognition in the model, we investigated intraneuronal Aβ deposition and tau pathology in treated and untreated 3xTg-AD mice. Intraneuronal Aβ deposits accumulate early (4 m.o.a.) in the 3xTg-AD hippocampus (Oddo et al., 2003). To verify whether pyruvate treatment has altered hippocampal Aβ deposition, we performed immunohistochemistry with the anti-Aβ DE2B4 primary antibody in the two study groups and found no significant Aβ reduction in treated 3xTg-AD mice (Fig. 2A-C, p=0.667).

12 m.o. 3xTg-AD mice develop tau pathology, first in the hippocampus (especially in CA1 pyramidal neurons) then in the cortex (Oddo et al., 2003). To investigate effects of pyruvate treatment on NFT development, we immunostained brain slices of the two study groups with the anti-tau AT180 primary antibody that specifically detects p-tau at the Thr231 site. Surprisingly, pyruvate administration increased p-tau immunoreactivity (Fig. 2D-F, p=0.035).

Pyruvate does not affect mitochondrial complex activity in 3xTg-AD brains

Mitochondrial dysfunction is a critical factor in age-related neurodegenerative diseases and AD in particular (Swerdlow and Khan, 2004; Lin and Beal, 2006; Crouch et al., 2007). To determine

whether pyruvate supplementation improves mitochondrial energy metabolism, we analyzed the activity of complex I, II, IV, and V in mitochondria isolated from the hippocampus and cortex of treated and untreated 3xTg-AD animals. Mitochondrial complexes were studied by means of BN-PAGE followed by histochemical in-gel staining. No statistically significant differences between the two study groups were found in the hippocampus (Fig. 3A: CI, p=0.442; CII, p=0.971; CIV, p=0.784; CV, p=0.439) or cortex (Fig. 3B: CI, p=0.706; CII, p=0.929; CIV, p=0.818; CV; p=0.657).

Pyruvate treatment does not change brain LDH activity and lactate levels in 3xTg-AD brains

Pyruvate may affect anaerobic glucose metabolism (Meany, 2007). In order to evaluate effects of pyruvate on this energetic pathway and potential interference with lactate, a molecule that has been recently shown to actively modulate the molecular determinants of long-term potentiation (Bouzier-Sore et al., 2003; Itoh et al., 2003; Suzuki et al., 2011), we measured forward ($LDH_{Pyr-Lac}$) and reverse ($LDH_{Lac-Pyr}$) LDH activities in brains of treated and untreated 3xTg-AD mice (Krieg et al., 1967). No significant differences were found between the two study groups for forward (p=0.087) or reverse (p=0.246) activities (Fig. 3C).

In the two study groups, we also evaluated lactate levels by GC-MS and found no significant differences (Fig. 3D, p=0.485).

Pyruvate supplementation does not influence the NAD^+: NADH ratio in 3xTg-AD brains

Pyruvate has been previously shown to restore the NAD^+ neuronal loss that is caused by neurotoxic $[Zn^{2+}]_i$ rises (Sheline et al., 2000). 3xTg-AD neurons have been shown to develop signs of oxidative stress dependent $[Zn^{2+}]_i$ dyshomeostasis (Sensi et al., 2008) and we therefore tested whether pyruvate supplementation modulates the NAD^+: NADH ratio in 3xTg-AD brains. Enzymatic assay revealed that treatment did not restore NAD^+ levels nor promoted changes in the NAD^+: NADH ratio (Fig. 3E, p=0.655).

Pyruvate treatment decreases lipid peroxidation in 3xTg-AD brains

Lipid peroxidation is an important index of neurodegeneration and has been described to be increased in 3xTg-AD brains (Resende et al., 2008). Lipid peroxidation was evaluated in 3xTg-AD brains with the TBARS assay to evaluate the *in vivo* antioxidant effects of pyruvate. TBARS analysis showed significant reduction in oxidative degradation of brain lipids in treated 3xTg-AD mice (Fig. 4, p=0.020).

Chronic pyruvate treatment decreases spontaneous Ca^{2+} spike frequency in 3xTg-AD neurons

Metabolic dysfunction and hyperexcitability have been shown to be causally related and administration of pyruvate in combination with 3-beta-hydroxybutyrate has been described to reduce epileptiform activity in a preclinical AD model (Pan et al., 2008; Kudin et al., 2009; Waldbaum and Patel, 2010; Zilberter et al., 2013). Given the enhanced neuronal excitability observed in 3xTg-AD mice *in vivo* (Davis et al., 2014), we explored whether the phenomenon could be attenuated by pyruvate. To gather information of pyruvate effects on the excitability of our Tg AD cultures, spontaneous activity was investigated in 3xTg-AD cultured neurons by measuring Ca^{2+} spikes. Ca^{2+} spikes were taken as an indirect index of synaptic activity occurring at baseline in the model. To that aim, 3xTg-AD cultured neurons were loaded with the high affinity Ca^{2+} indicator Fluo-4 (K_d= 345 nM) and spontaneous fluctuations of $[Ca^{2+}]_i$ measured and analyzed in terms of changes in spike frequencies and amplitudes. A pre-incubation of 3 days with 10 mM pyruvate, also kept in the medium throughout the imaging experiment, showed that, compared to sham-washed cultures, treated cultures exhibited significant spike frequency reductions (Fig. 5A, B, $p<1*10^{-4}$) coupled with increases in spike amplitude (Fig. 5A, C, $p<1*10^{-4}$).

Chronic pyruvate treatment attenuates ROS levels in 3xTg-AD neurons

Considering the close relationship between Ca^{2+} deregulation and ROS generation, we then investigated whether long-term (3 days) pyruvate treatment could result in reduction of oxidative stress in 3xTg-AD neurons. Intracellular ROS levels were microfluorimetrically studied in cultured 3xTg-AD neurons loaded with HEt, a superoxide-sensitive fluorescent indicator. In cultures treated before and during the experiment with 10 mM pyruvate, HEt imaging revealed that, compared to sham-washed cultures, the molecule promoted a significant decrease in baseline levels of ROS in 3xTg-AD neurons (Fig. 6A, p=0.013).

Pyruvate modulates $[Zn^{2+}]_i$ and $[Ca^{2+}]_i$ levels in 3xTg-AD neurons

ROS production is a potent trigger for mobilization of $[Zn^{2+}]_i$, a critical mediator of neuronal death (Sensi et al., 2003, 2009; Aras and Aizenman, 2011), and a phenomenon found distinctively increased in 3xTg-AD neurons (Sensi et al.,2008). We therefore, investigated whether pyruvate affects ROS-driven $[Zn^{2+}]_i$ elevations in cultured 3xTg-AD neurons. To that aim, 3xTg-AD neurons challenged with the cell oxidant DTDP, a maneuver that promotes $[Zn^{2+}]_i$ rises by mobilizing the

cation from metallothioneins (Sensi et al., 2008; Aras and Aizenman, 2011). $[Zn^{2+}]_i$ changes were investigated in cultured neurons loaded with the Zn^{2+}-selective fluorescent probe FluoZin-3 (K_d= 15 nM) and undergoing a 20 minutes exposure to 25 µM DTDP. 10 mM pyruvate, pre-incubated for 30 minutes before DTDP exposure and kept during the whole experiment, was found to significantly decrease DTDP-dependent $[Zn^{2+}]_i$ rises in treated cultures (Fig. 6B, C; p=0.035).

ROS-dependent $[Zn^{2+}]_i$ mobilization can also affect $[Ca^{2+}]_i$ homeostasis. As glutamatergic overdrive is a major trigger for Ca^{2+}- dependent ROS production (Dugan et al., 1995; Reynolds and Hastings, 1995), we evaluated whether pyruvate synergistically affects levels of the two cations in neurons challenged with an excitotoxic paradigm.

To that aim, glutamate-dependent cation rises in 3xTg-AD neurons were evaluated in cultures undergoing a 3 days pre-incubation with 10 mM pyruvate prior to 10 minutes NMDA exposure (50 µM + glycine 15 µM) and compared to sham-washed control cultures. Pyruvate treated 3xTg-AD neurons loaded with the low affinity Ca^{2+} indicator Fluo-4FF, showed a significant decrease in NMDA-driven $[Ca^{2+}]_i$ rises when compared to controls (Fig. 7A, B; $p=1*10^{-4}$).

As for Zn^{2+}, pyruvate treatment significantly reduced NMDA-driven $[Zn^{2+}]_i$ mobilization from intracellular pools in FluoZin-3 loaded neurons (Fig. 7C, D; $p=1*10^{-4}$). The effect was not dependent on the length of pre-incubation time as the inhibition reached a plateau within 30 minutes of pre-treatment (data not shown) and was not further enhanced by a more prolonged (7 day) compound exposure (data not shown).

Discussion

The aim of this study was to investigate neuroprotective effects of chronic administration of pyruvate in a preclinical model of AD. Previous studies in rats subjected to insulin-induced hypoglycemia or traumatic brain injury have demonstrated positive pyruvate effects on memory function (Suh et al., 2005; Moro et al., 2011). We confirmed effects in short and long-term memory performances in treated 3xTg-AD mice. To our knowledge, this is the first study showing a beneficial role for pyruvate on a preclinical AD model.

To assess whether these positive cognitive effects are associated with decreased amyloid and tau deposition, we compared brain levels of the two AD hallmarks in the study groups. Interestingly, no reductions in amyloid or p-tau deposition were observed. This result, although unexpected, is in accordance with evidence indicating that neuroprotective intervention like

neural stem cell transplantation or activation of neurotrophic pathways by $p75^{NTR}$ can halt or rescue the development of cognitive deficits without interfering with amyloid and/or tau-pathology of transgenic AD models (Blurton-Jones et al., 2009; Knowles et al., 2013).

Even more surprising was the drug effect on p-tau as treated 3xTg-AD mice showed increased hippocampal levels of p-tau deposits. This result is not in line with many studies that have demonstrated a positive correlation between preservation of cognitive performances and reduction of p-tau levels (Corona et al., 2010; LaFerla, 2010; Fuso et al., 2012; Huang and Mucke, 2012). A possible partial explanation comes from recent evidence that indicates the possibility of a more complex scenario in which tau appears to exert much of the damage when present in monomeric configuration outside of neurons rather than when inside in form of NFT aggregates (Michel et al., 2014). The paradoxical increase in p-tau can be also explained in view of recent findings showing that, in brain slice cultures, pyruvate inhibits protein phosphatase 2A activity (Wang et al., 2012). Protein phosphatase 2A plays a pivotal role in tau dephosphorylation and is down-regulated in AD brains (Gong and Iqbal, 2008). Protein phosphatase 2A can dephosphorylate tau at multiple sites (Wang et al., 2013) including Thr231, the site recognized by the AT180 antibody employed in this study. Thus, increased p-tau levels observed in treated 3xTg-AD mice can be linked to a pyruvate-dependent inhibition of tau dephosphorylation at the Thr231 site. Protein phosphatase 2A is also activated by ROS. Pyruvate, acting as antioxidant, can therefore affect the enzyme activity by quenching oxidative stress (Wang et al., 2012).

Pyruvate is known to be an important energy substrate that fuels glycolysis. We have therefore evaluated brain metabolic pathways in which the compound is involved. To that aim, we investigated the intracellular fate of pyruvate and studied effects on 3xTg-AD brain aerobic and anaerobic pathways.

Brain mitochondria have been described to be functionally impaired in 3xTg-AD mice (Corona et al., 2010, 2011a). At first, we evaluated effects of pyruvate on mitochondrial complexes of 3xTg-AD hippocampi and cortices and found no changes in the activity of complex I, II, IV, and V. We then investigated effects of pyruvate administration on anaerobic glycolytic pathways by evaluating forward ($LDH_{Pyr\text{-}Lac}$) and reverse ($LDH_{Lac\text{-}Pyr}$) brain LDH activities. Brain anaerobic glycolysis is strictly related to the astrocyte-neuron lactate shuttle system, the astrocyte-neuron interplay based on neuronal uptake of lactate that is released from astrocytes (Pellerin and Magistretti, 2012). Lactate is not only a neuronal energy substrate but also critical for cognition by promoting neuronal plasticity and the maintenance of long-term potentiation

(Bouzier-Sore et al., 2003; Itoh et al., 2003; Suzuki et al., 2011). No differences were found in both enzymatic activities between the two study groups. This result was confirmed by levels of brain lactate in mice supplemented with pyruvate that were comparable to the ones found in untreated mice.

In line with these data, brains of treated 3xTg-AD mice did not show significant changes on the NAD^+: NADH ratio. Our data are not in accordance with previous *in vitro* observations obtained in cortical neurons (Sheline et al., 2010) indicating that pyruvate counteracts NAD^+ decreases resulting from neurotoxic Zn^{2+} exposures. This discrepancy likely reflects the higher level of complexity offered by the *in vivo* 3xTg-AD mouse model when compared to the more homogenous scenario represented by cultured neurons obtained from non-transgenic animals. A decrease in NAD^+: NADH ratio is associated with aging progression, and NAD^+ level increase can counteract mitochondrial dysfunction in old mice (Gomes et al., 2013). Pyruvate treatment did not restore the NAD^+: NADH ratio in 3xTg-AD mice, thereby supporting the idea of negligible effects on mitochondrial complex activity. In summary, this set of experiments rules out a major effect of pyruvate on brain metabolism.

In search for the molecular determinants of the beneficial cognitive effects, we have then investigated pyruvate antioxidant properties as the compound can act as ROS scavenger. *In vivo,* pyruvate treatment improves the brain redox state (Mongan et al., 2002, 2003) and, *in vitro*, the molecule suppresses ROS production in neuronal cultures exposed to neurotoxic insults (Desagher et al., 1997; Alvarez et al., 2003; Chen and Liao, 2003). Pyruvate also reduces H_2O_2 through non-enzymatic decarboxylation (Desagher et al., 1997). We have therefore evaluated effects on brain lipid peroxidation, a marker of oxidative stress that is increased in 3xTg-AD mice (Resende et al., 2008). In this set of experiments, with a potential caveat due to the low sample size, we found that TBARS levels were significantly decreased in pyruvate-treated 3xTg-AD mice (Fig. 4). ROS generation promotes membrane lipid peroxidation that is also an important step in the excitotoxic cascade (Blanc et al., 1998; Lauderback et al., 2001), a main trait of AD that is centered on Ca^{2+}-dependent generation of oxidative stress (Choi, 1988; Dugan et al., 1995).

Glutamate, oxidative stress, and AD can be linked in the context of neuronal hyperexcitability. Hyperexcitability has been described in AD models and patients and can be the trigger for glutamatergic overstimulation (Palop and Mucke, 2009; Noebels, 2011; Friedman et al., 2012; Davis et al., 2014). Pyruvate, in association with 3-beta-hydroxybutyrate, has been shown to reduce epileptiform activity in a AD mouse model (Zilberter et al., 2013). In line with this set of

data, we observed a significant reduction of spontaneous synaptic activity as indicated by decreased $[Ca^{2+}]_i$ spike frequency in pyruvate-treated 3xTg-AD cultured neurons (Fig. 5A-C). Our results indicate that pyruvate by itself is sufficient to decrease altered spontaneous synaptic activity in 3xTg-AD treated neuronal cultures.

As glutamate receptor overactivation can lead to enhanced oxidative stress, we then investigated ROS levels in 3xTg-AD neurons chronically exposed to pyruvate in comparison to untreated cultures. This set of experiments showed that chronic pyruvate exposure was able to reduce baseline oxidative stress levels (Fig. 6A), thereby indicating that the compound can cumulatively act in the direction of reducing oxidative stress possibly by combining direct antioxidant properties with a reduction of glutamatergic hyperexcitability and subsequent glutamate-dependent ROS generation. Our in vitro results are in line with the in vivo dataset on brain lipid peroxidation. With the limitation of the low number of brain samples that we had left to be assayed, we found that pyruvate shows inhibitory effects on lipoperoxidation, an overall endpoint that can be regarded as indicative of an undergoing increased oxidative stress occurring in the animal model. In the in vitro experiment, we chose a condition (long-term, 3 day, pyruvate pre-incubation) that aimed at mimicking the chronic pyruvate treatment we employed in 3xTg-AD animals. Thus, with the limitation we have underlined, the positive in vitro effects are conceptually in line with the general antioxidant results found in vivo and support the hypothesis that reduction of oxidative stress is an important mechanistic component of the neuroprotection operated by pyruvate.

ROS generation can trigger injurious mobilization of $[Zn^{2+}]_i$ and our transgenic model has been described to exhibit deregulated $[Zn^{2+}]_i$ levels upon conditions of oxidative stress (Sensi et al., 2008). Furthermore, Zn^{2+} deregulation can synergistically act with Ca^{2+} to produce injury since glutamate-driven ROS production mobilizes $[Zn^{2+}]$. This phenomenon promotes mitochondrial dysfunction and further increases ROS production, thereby generating a potentially self-perpetuating pathogenic loop (Corona et al., 2011b). Zn^{2+} deregulation occurring in the disease helps to explain the some of the mechanism involved in synaptic dysfunction and cognitive decline associated with AD development and progression (Demuro et al., 2010; Corona et al., 2011b; Craddock et al., 2012; Roberts et al., 2012; Bush, 2013).

With this conceptual framework as rationale, we tested whether pyruvate affects glutamate-driven deregulation of intraneuronal $[Zn^{2+}]_i$ and $[Ca^{2+}]_i$. Using real-time single cell Zn^{2+} and Ca^{2+} imaging in 3xTg-AD cultures that were challenged with excitotoxic stimuli, we found that

the compound reduced Ca^{2+} and Zn^{2+} dyshomeostasis elicited by N-methyl-D-aspartate receptor (NMDARs) activation (Fig. 7A-D).

Supporting the hypothesis that pyruvate can halt the Ca^{2+}/ROS/Zn^{2+} vicious cycle by decreasing ROS-dependent $[Zn^{2+}]_i$ mobilization, the compound was also found to significantly reduce $[Zn^{2+}]_i$ rises triggered by DTDP (Fig. 6B, C). The effect was unlikely to be related to direct Zn^{2+} chelation given the molecule low log stability constant for the ion (1.3; Martell and Smith, 1995). Pyruvate effects on ROS and Zn^{2+} may have reverberating beneficial effects on mitochondrial functioning and on the organelle capability to handle $[Ca^{2+}]_i$, thereby interrupting a self-enhancing cycle of cation deregulation and oxidative stress.

Our findings are not in line with previous data on wild type cultured cortical neurons showing that pyruvate does not counteract ROS-dependent $[Zn^{2+}]_i$ rises (Sheline et al., 2010). This discrepancy can be explained by differences in experimental protocols and setups as we used an excitotoxic stimulus, performed pre-incubation with pyruvate instead of acute co-exposures and employed transgenic AD cultures instead of non-transgenic neurons. The difference between non-Tg and 3xTg-AD mice seems to be particularly important given the higher level of ROS-dependent $[Zn^{2+}]_i$ deregulation that we have described in cortical neurons obtained from this AD model (Sensi et al., 2008).

Conclusions

Overall, our study indicates that pyruvate counteracts the development of cognitive decline in the 3xTg-AD mouse model. These beneficial effects appear to be more dependent on the compound activity on neuronal hyperexcitability and spontaneous synaptic activity, oxidative stress as well as glutamate-driven deregulation of $[Ca^{2+}]_i$ and $[Zn^{2+}]_i$ levels rather than on modulation of energy metabolism.

Interestingly, these pro-cognitive effects are achieved without reductions in amyloid- and tau-dependent pathology, thereby suggesting that pyruvate mediates inhibition of additional pathogenic pathways. Pyruvate therefore has the potential to be implemented as safe and inexpensive therapeutic agent that can work in a complementary fashion along with drugs that more directly address Aβ and tau-dependent pathogenic mechanisms.

Acknowledgments

SLS is supported by funds from the Italian Department of Education (PRIN, 2008 and 2011) and the “Marisa Trampuz von Langendorf” Fellowship for Neuroscience.

References

Alvarez G, Ramos M, Ruiz F, Satrústegui J, Bogónez E (2003) Pyruvate protection against beta-amyloid-induced neuronal death: role of mitochondrial redox state. J Neurosci Res 73:260–269.

Aras MA, Aizenman E (2011) Redox regulation of intracellular zinc: molecular signaling in the life and death of neurons. Antioxid Redox Signal 15:2249–2263.

Bakker A, Krauss GL, Albert MS, Speck CL, Jones LR, Stark CE, Yassa MA, Bassett SS, Shelton AL, Gallagher M (2012) Reduction of Hippocampal Hyperactivity Improves Cognition in Amnestic Mild Cognitive Impairment. Neuron 74:467–474.

Billings LM, Oddo S, Green KN, McGaugh JL, LaFerla FM (2005) Intraneuronal Abeta causes the onset of early Alzheimer’s disease-related cognitive deficits in transgenic mice. Neuron 45:675–688.

Blanc EM, Keller JN, Fernandez S, Mattson MP (1998) 4-hydroxynonenal, a lipid peroxidation product, impairs glutamate transport in cortical astrocytes. Glia 22:149–160.

Blurton-Jones M, Kitazawa M, Martinez-Coria H, Castello NA, Müller F-J, Loring JF, Yamasaki TR, Poon WW, Green KN, LaFerla FM (2009) Neural stem cells improve cognition via BDNF in a transgenic model of Alzheimer disease. Proc Natl Acad Sci U S A 106:13594–13599.

Bomba M, Ciavardelli D, Silvestri E, Canzoniero LMT, Lattanzio R, Chiappini P, Piantelli M, Di Ilio C, Consoli A, Sensi SL (2013) Exenatide promotes cognitive enhancement and positive brain metabolic changes in PS1-KI mice but has no effects in 3xTg-AD animals. Cell Death Dis 4:e612.

Bouzier-Sore A-K, Voisin P, Canioni P, Magistretti PJ, Pellerin L (2003) Lactate is a preferential oxidative energy substrate over glucose for neurons in culture. J Cereb Blood Flow Metab Off J Int Soc Cereb Blood Flow Metab 23:1298–1306.

Bush AI (2013) The metal theory of Alzheimer’s disease. J Alzheimers Dis JAD 33 Suppl 1:S277–S281.

Canzoniero LMT, Granzotto A, Turetsky DM, Choi DW, Dugan LL, Sensi SL (2013) nNOS(+) striatal neurons, a subpopulation spared in Huntington’s Disease, possess functional NMDA receptors but fail to generate mitochondrial ROS in response to an excitotoxic challenge. Front Physiol 4:112.

Chakroborty S, Kim J, Schneider C, Jacobson C, Molgó J, Stutzmann GE (2012) Early presynaptic and postsynaptic calcium signaling abnormalities mask underlying synaptic depression in presymptomatic Alzheimer’s disease mice. J Neurosci Off J Soc Neurosci 32:8341–8353.

Chen C-J, Liao S-L (2003) Zinc toxicity on neonatal cortical neurons: involvement of glutathione chelation. J Neurochem 85:443–453.

Choi BY, Kim JH, Kim HJ, Yoo JH, Song HK, Sohn M, Won SJ, Suh SW (2013) Pyruvate administration reduces recurrent/moderate hypoglycemia-induced cortical neuron death in diabetic rats. PloS One 8:e81523.

Choi DW (1988) Glutamate neurotoxicity and diseases of the nervous system. Neuron 1:623–634.

Corona C, Frazzini V, Silvestri E, Lattanzio R, La Sorda R, Piantelli M, Canzoniero LMT, Ciavardelli D, Rizzarelli E, Sensi SL (2011a) Effects of dietary supplementation of carnosine on mitochondrial dysfunction, amyloid pathology, and cognitive deficits in 3xTg-AD mice. PloS One 6:e17971.

Corona C, Masciopinto F, Silvestri E, Viscovo AD, Lattanzio R, Sorda RL, Ciavardelli D, Goglia F, Piantelli M, Canzoniero LMT, Sensi SL (2010) Dietary zinc supplementation of 3xTg-AD mice increases BDNF levels and prevents cognitive deficits as well as mitochondrial dysfunction. Cell Death Dis 1:e91.

Corona C, Pensalfini A, Frazzini V, Sensi SL (2011b) New therapeutic targets in Alzheimer's disease: brain deregulation of calcium and zinc. Cell Death Dis 2:e176.

Craddock TJA, Tuszynski JA, Chopra D, Casey N, Goldstein LE, Hameroff SR, Tanzi RE (2012) The zinc dyshomeostasis hypothesis of Alzheimer's disease. PloS One 7:e33552.

Crouch PJ, Cimdins K, Duce JA, Bush AI, Trounce IA (2007) Mitochondria in aging and Alzheimer's disease. Rejuvenation Res 10:349–357.

Davis KE, Fox S, Gigg J (2014) Increased hippocampal excitability in the 3xTgAD mouse model for Alzheimer's disease in vivo. PloS One 9:e91203.

Demuro A, Parker I, Stutzmann GE (2010) Calcium signaling and amyloid toxicity in Alzheimer disease. J Biol Chem 285:12463–12468.

Desagher S, Glowinski J, Prémont J (1997) Pyruvate protects neurons against hydrogen peroxide-induced toxicity. J Neurosci Off J Soc Neurosci 17:9060–9067.

Dugan LL, Sensi SL, Canzoniero LM, Handran SD, Rothman SM, Lin TS, Goldberg MP, Choi DW (1995) Mitochondrial production of reactive oxygen species in cortical neurons following exposure to N-methyl-D-aspartate. J Neurosci Off J Soc Neurosci 15:6377–6388.

Friedman D, Honig LS, Scarmeas N (2012) Seizures and epilepsy in Alzheimer's disease. CNS Neurosci Ther 18:285–294.

Fukushima M, Lee SM, Moro N, Hovda DA, Sutton RL (2009) Metabolic and histologic effects of sodium pyruvate treatment in the rat after cortical contusion injury. J Neurotrauma 26:1095–1110.

Fuso A, Nicolia V, Ricceri L, Cavallaro RA, Isopi E, Mangia F, Fiorenza MT, Scarpa S (2012) S-adenosylmethionine reduces the progress of the Alzheimer-like features induced by B-vitamin deficiency in mice. Neurobiol Aging 33:1482.e1–e16.

Gatta V, D'Aurora M, Granzotto a, Stuppia L, Sensi SL (2014) Early and sustained altered expression of aging-related genes in young 3xTg-AD mice. Cell Death Dis 5:e1054.

Gomes AP, Price NL, Ling AJY, Moslehi JJ, Montgomery MK, Rajman L, White JP, Teodoro JS, Wrann CD, Hubbard BP, Mercken EM, Palmeira CM, de Cabo R, Rolo AP, Turner N, Bell EL, Sinclair DA (2013) Declining

NAD(+) induces a pseudohypoxic state disrupting nuclear-mitochondrial communication during aging. Cell 155:1624–1638.

Gong C-X, Iqbal K (2008) Hyperphosphorylation of microtubule-associated protein tau: a promising therapeutic target for Alzheimer disease. Curr Med Chem 15:2321–2328.

Gramsbergen JB, Sandberg M, Kornblit B, Zimmer J (2000) Pyruvate protects against 3-nitropropionic acid neurotoxicity in corticostriatal slice cultures. Neuroreport 11:2743–2747.

Hardy JA, Higgins GA (1992) Alzheimer's disease: the amyloid cascade hypothesis. Science 256:184–185.

Hardy J, Selkoe DJ (2002) The amyloid hypothesis of Alzheimer's disease: progress and problems on the road to therapeutics. Science 297:353–356.

Huang Y, Mucke L (2012) Alzheimer mechanisms and therapeutic strategies. Cell 148:1204–1222.

Itoh Y, Esaki T, Shimoji K, Cook M, Law MJ, Kaufman E, Sokoloff L (2003) Dichloroacetate effects on glucose and lactate oxidation by neurons and astroglia in vitro and on glucose utilization by brain in vivo. Proc Natl Acad Sci U S A 100:4879–4884.

Ittner LM, Götz J (2011) Amyloid-β and tau--a toxic pas de deux in Alzheimer's disease. Nat Rev Neurosci 12:65–72.

Izumi Y, Zorumski CF (2010) Neuroprotective effects of pyruvate following NMDA-mediated excitotoxic insults in hippocampal slices. Neurosci Lett 478:131–135.

Jones KA, Baughman RW (1991) Both NMDA and non-NMDA subtypes of glutamate receptors are concentrated at synapses on cerebral cortical neurons in culture. Neuron 7:593–603.

Knowles JK, Simmons DA, Nguyen T-VV, Vander Griend L, Xie Y, Zhang H, Yang T, Pollak J, Chang T, Arancio O, Buckwalter MS, Wyss-Coray T, Massa SM, Longo FM (2013) Small molecule p75NTR ligand prevents cognitive deficits and neurite degeneration in an Alzheimer's mouse model. Neurobiol Aging 34:2052–2063.

Krieg AF, Rosenblum LJ, Henry JB (1967) Lactate dehydrogenase isoenzymes a comparison of pyruvate-to-lactate and lactate-to-pyruvate assays. Clin Chem 13:196–203.

Kudin AP, Zsurka G, Elger CE, Kunz WS (2009) Mitochondrial involvement in temporal lobe epilepsy. Exp Neurol 218:326–332.

LaFerla FM (2010) Pathways linking Abeta and tau pathologies. Biochem Soc Trans 38:993–995.

Lauderback CM, Hackett JM, Huang FF, Keller JN, Szweda LI, Markesbery WR, Butterfield DA (2001) The glial glutamate transporter, GLT-1, is oxidatively modified by 4-hydroxy-2-nonenal in the Alzheimer's disease brain: the role of Abeta1-42. J Neurochem 78:413–416.

Lee JY, Kim YH, Koh JY (2001) Protection by pyruvate against transient forebrain ischemia in rats. J Neurosci Off J Soc Neurosci 21:RC171.

Li JH, Wang YH, Wolfe BB, Krueger KE, Corsi L, Stocca G, Vicini S (1998) Developmental changes in localization of NMDA receptor subunits in primary cultures of cortical neurons. Eur J Neurosci 10:1704–1715.

Lin MT, Beal MF (2006) Mitochondrial dysfunction and oxidative stress in neurodegenerative diseases. Nature 443:787–795.

Masciopinto F, Di Pietro N, Corona C, Bomba M, Pipino C, Curcio M, Di Castelnuovo A, Ciavardelli D, Silvestri E, Canzoniero LMT, Sekler I, Pandolfi A, Sensi SL (2012) Effects of long-term treatment with pioglitazone on cognition and glucose metabolism of PS1-KI, 3xTg-AD, and wild-type mice. Cell Death Dis 3:e448.

Maus M, Marin P, Israël M, Glowinski J, Prémont J (1999) Pyruvate and lactate protect striatal neurons against N-methyl-D-aspartate-induced neurotoxicity. Eur J Neurosci 11:3215–3224.

Meany JE (2007) Lactate Dehydrogenase Catalysis: Roles of Keto, Hydrated, and Enol Pyruvate. J Chem Educ 84:1520–1523.

Michel CH, Kumar S, Pinotsi D, Tunnacliffe A, St George-Hyslop P, Mandelkow E, Mandelkow E-M, Kaminski CF, Kaminski Schierle GS (2014) Extracellular monomeric tau protein is sufficient to initiate the spread of tau protein pathology. J Biol Chem 289:956–967.

Miller LP, Oldendorf WH (1986) Regional kinetic constants for blood-brain barrier pyruvic acid transport in conscious rats by the monocarboxylic acid carrier. J Neurochem 46:1412–1416.

Mongan PD, Capacchione J, West S, Karaian J, Dubois D, Keneally R, Sharma P (2002) Pyruvate improves redox status and decreases indicators of hepatic apoptosis during hemorrhagic shock in swine. Am J Physiol Heart Circ Physiol 283:H1634–H1644.

Mongan PD, Karaian J, Van Der Schuur BM, Via DK, Sharma P (2003) Pyruvate prevents poly-ADP ribose polymerase (PARP) activation, oxidative damage, and pyruvate dehydrogenase deactivation during hemorrhagic shock in swine. J Surg Res 112:180–188.

Moro N, Ghavim SS, Hovda DA, Sutton RL (2011) Delayed sodium pyruvate treatment improves working memory following experimental traumatic brain injury. Neurosci Lett 491:158–162.

Noebels J (2011) A perfect storm: Converging paths of epilepsy and Alzheimer's dementia intersect in the hippocampal formation. Epilepsia 52 Suppl 1:39–46.

Oddo S, Caccamo A, Shepherd JD, Murphy MP, Golde TE, Kayed R, Metherate R, Mattson MP, Akbari Y, LaFerla FM (2003) Triple-transgenic model of Alzheimer's disease with plaques and tangles: intracellular Abeta and synaptic dysfunction. Neuron 39:409–421.

Palop JJ, Mucke L (2009) Epilepsy and cognitive impairments in Alzheimer disease. Arch Neurol 66:435–440.

Pan JW, Cavus I, Kim J, Hetherington HP, Spencer DD (2008) Hippocampal extracellular GABA correlates with metabolism in human epilepsy. Metab Brain Dis 23:457–468.

Pellerin L, Magistretti PJ (2012) Sweet sixteen for ANLS. J Cereb Blood Flow Metab Off J Int Soc Cereb Blood Flow Metab 32:1152–1166.

Resende R, Moreira PI, Proença T, Deshpande A, Busciglio J, Pereira C, Oliveira CR (2008) Brain oxidative stress in a triple-transgenic mouse model of Alzheimer disease. Free Radic Biol Med 44:2051–2057.

Reynolds IJ, Hastings TG (1995) Glutamate induces the production of reactive oxygen species in cultured forebrain neurons following NMDA receptor activation. J Neurosci Off J Soc Neurosci 15:3318–3327.

Roberts BR, Ryan TM, Bush AI, Masters CL, Duce JA (2012) The role of metallobiology and amyloid-β peptides in Alzheimer's disease. J Neurochem 120 Suppl 1:149–166.

Schägger H, Bentlage H, Ruitenbeek W, Pfeiffer K, Rotter S, Rother C, Böttcher-Purkl A, Lodemann E (1996) Electrophoretic separation of multiprotein complexes from blood platelets and cell lines: technique for the analysis of diseases with defects in oxidative phosphorylation. Electrophoresis 17:709–714.

Sensi SL, Canzoniero LM, Yu SP, Ying HS, Koh JY, Kerchner GA, Choi DW (1997) Measurement of intracellular free zinc in living cortical neurons: routes of entry. J Neurosci Off J Soc Neurosci 17:9554–9564.

Sensi SL, Paoletti P, Bush AI, Sekler I (2009) Zinc in the physiology and pathology of the CNS. Nat Rev Neurosci 10:780–791.

Sensi SL, Rapposelli IG, Frazzini V, Mascetra N (2008) Altered oxidant-mediated intraneuronal zinc mobilization in a triple transgenic mouse model of Alzheimer's disease. Exp Gerontol 43:488–492.

Sensi SL, Ton-That D, Sullivan PG, Jonas EA, Gee KR, Kaczmarek LK, Weiss JH (2003) Modulation of mitochondrial function by endogenous Zn2+ pools. Proc Natl Acad Sci U S A 100:6157–6162.

Sensi SL, Yin HZ, Carriedo SG, Rao SS, Weiss JH (1999a) Preferential Zn2+ influx through Ca2+-permeable AMPA/kainate channels triggers prolonged mitochondrial superoxide production. Proc Natl Acad Sci U S A 96:2414–2419.

Sensi SL, Yin HZ, Weiss JH (1999b) Glutamate triggers preferential Zn2+ flux through Ca2+ permeable AMPA channels and consequent ROS production. Neuroreport 10:1723–1727.

Sheline CT, Behrens MM, Choi DW (2000) Zinc-induced cortical neuronal death: contribution of energy failure attributable to loss of NAD(+) and inhibition of glycolysis. J Neurosci Off J Soc Neurosci 20:3139–3146.

Sheline CT, Cai A-L, Zhu J, Shi C (2010) Serum or target deprivation-induced neuronal death causes oxidative neuronal accumulation of Zn2+ and loss of NAD+. Eur J Neurosci 32:894–904.

Stanika RI, Pivovarova NB, Brantner CA, Watts CA, Winters CA, Andrews SB (2009) Coupling diverse routes of calcium entry to mitochondrial dysfunction and glutamate excitotoxicity. Proc Natl Acad Sci U S A 106:9854–9859.

Suh SW, Aoyama K, Matsumori Y, Liu J, Swanson RA (2005) Pyruvate administered after severe hypoglycemia reduces neuronal death and cognitive impairment. Diabetes 54:1452–1458.

Sutherland RJ, McDonald RJ (1990) Hippocampus, amygdala, and memory deficits in rats. Behav Brain Res 37:57–79.

Suzuki A, Stern SA, Bozdagi O, Huntley GW, Walker RH, Magistretti PJ, Alberini CM (2011) Astrocyte-neuron lactate transport is required for long-term memory formation. Cell 144:810–823.

Swerdlow RH, Khan SM (2004) A "mitochondrial cascade hypothesis" for sporadic Alzheimer's disease. Med Hypotheses 63:8–20.

Vossel K a, Beagle AJ, Rabinovici GD, Shu H, Lee SE, Naasan G, Hegde M, Cornes SB, Henry ML, Nelson AB, Seeley WW, Geschwind MD, Gorno-Tempini ML, Shih T, Kirsch HE, Garcia P a, Miller BL, Mucke L (2013) Seizures and epileptiform activity in the early stages of Alzheimer disease. JAMA Neurol 70:1158–1166.

Waldbaum S, Patel M (2010) Mitochondria, oxidative stress, and temporal lobe epilepsy. Epilepsy Res 88:23–45.

Wang J-Z, Xia Y-Y, Grundke-Iqbal I, Iqbal K (2013) Abnormal hyperphosphorylation of tau: sites, regulation, and molecular mechanism of neurofibrillary degeneration. J Alzheimers Dis JAD 33 Suppl 1:S123–S139.

Wang X, Takata T, Bai X, Ou F, Yokono K, Sakurai T (2012) Pyruvate prevents the inhibition of the long-term potentiation induced by amyloid-β through protein phosphatase 2A inactivation. J Alzheimers Dis JAD 30:665–673.

Yoo MH, Lee J-Y, Lee SE, Koh J-Y, Yoon YH (2004) Protection by pyruvate of rat retinal cells against zinc toxicity in vitro, and pressure-induced ischemia in vivo. Invest Ophthalmol Vis Sci 45:1523–1530.

Zilberter M, Ivanov A, Ziyatdinova S, Mukhtarov M, Malkov A, Alpár A, Tortoriello G, Botting CH, Fülöp L, Osypov AA, Pitkänen A, Tanila H, Harkany T, Zilberter Y (2013) Dietary energy substrates reverse early neuronal hyperactivity in a mouse model of Alzheimer's disease. J Neurochem 125:157–171.

Figure legends

Figure 1 *Pyruvate treatment rescues hippocampal-dependent short- and long-term memory deficits in 3xTg-AD mice*.

Untreated (6 m.o.a. n=18; 12 m.o.a. n=19) and treated (6 m.o.a. n=27; 12 m.o.a. n=22) 3xTg-AD mice were tested for memory performance with the MWM test. (**A**, **C**) Animals were evaluated 1.5 h after the last training session to investigate short-term memory. (**A**) Analysis of crosses (the number of times the mouse crosses platform location) showed statistically significant increases in treated 3xTg-AD mice at 6 m.o.a. (p=0.038) or 12 m.o.a. (p=0.041) when compared to age-matched untreated mice. (**C**) Analysis of latency (the time spent to reach the point where the platform used to be) indicated statistically significant improvements in treated mice only at 12 m.o.a. (p=0.034). (**B**, **D**) Animals were evaluated 24 h after the last training session to investigate long-term memory. (**B**) Analysis of crosses showed statistically significant increases in treated 3xTg-AD mice at 6 m.o.a. (p=0.013) when compared to age-matched untreated mice. (**D**) Analysis of latency indicated statistically significant improvements in treated mice only at 12 m.o.a. (p=0.017). Bars show mean (± S.E.M.) values; *$p \leq 0.05$.

Figure 2 *Pyruvate treatment does not affect intraneuronal* Aβ *deposition while enhances p-tau levels in the hippocampus of 12 m.o. 3xTg-AD mice.*

Immunohistochemistry was employed to detect deposits of intraneuronal Aβ (**A**-**C**) and p-tau (**D**-**F**) in brain slices from treated and untreated 3xTg-AD mice. (**A**, **B**) Aβ-immunohistochemical staining in the hippocampus of treated (n=12) and untreated (n=11) 3xTg-AD mice did not show statistically significant differences between the two groups (quantified in **C**). (**D**, **E**) Compared to untreated mice (n=10), treated 3xTg-AD mice (n=12) showed increased p-tau (Thr231) immunoreactivity (p=0.035; quantified in **F**). anels depict images with a 10x magnification (scale bar=100 μm). Insets show high (40x) magnification views of the hippocampal CA1 subregion (scale bar=20 μm). Bars show mean (± S.E.M.) values; *$p \leq 0.05$.

Figure 3 *Pyruvate treatment has no effect on aerobic and anaerobic glycolysis*.

Pyruvate effect on aerobic glycolysis was investigated by employing BN-PAGE to evaluate the activity of mitochondrial complex I, II, IV and V on hippocampi (**A**) and cortices (**B**) of treated and untreated 3xTg-AD mice (n=6 per group). (**A**, **B**) Pyruvate treatment did not change Alzheimer's disease-related mitochondrial complex functioning neither on hippocampi nor on cortices. Pyruvate effect on anaerobic glycolysis was investigated by employing spectrophotometric evaluation of LDH activities, GC-MS measurement of lactate levels and assessment of NAD^+: NADH ratio with a commercially available assay kit in brains from treated and untreated 3xTg-AD mice (n=3 per group). (**C**) Pyruvate treatment showed no effect on forward (left) or reverse (right) LDH activities. (**D**) The lactate levels measurement showed that pyruvate supplementation had no effects on this parameter. (**E**) Pyruvate treatment did not change the NAD^+: NADH ratio between the two study groups. Bars show mean (± S.E.M.) values.

Figure 4 *Pyruvate treatment decreases lipid peroxidation in 3xTg-AD brains.*

TBARS assay was employed to evaluate lipid peroxidation in 3xTg-AD brains. Treated (n=3) mice showed significant reduction in TBARS levels (p=0.020) when compared to untreated animals (n=2). Bars show mean (± S.E.M.) values.; *$p \leq 0.05$.

Figure 5 *Chronic pyruvate treatment reduces spontaneous synaptic activity in 3xTg-AD neurons.*

Analysis of spontaneous $[Ca^{2+}]_i$ rises assessed with the high affinity Ca^{2+} indicator Fluo-4. (**A**) Representative traces of Ca^{2+} spikes in untreated (blue trace) and pyruvate treated (red trace) 3xTg-AD neurons. (**B**, **C**) Spontaneous $[Ca^{2+}]_i$ rises were evaluated for up to 5 min with a 2 Hz sampling rate. Quantification of $[Ca^{2+}]_i$ spike frequency (**B**) and amplitude (**C**) in untreated cultures (n=231 neurons from 4 independent experiments) were compared with those of occurring in pyruvate treated cultures (n=231 neurons from 4 independent experiments). Pyruvate treatment promoted a significant reduction of spike frequency ($p<1*10^{-4}$; **B**) and a significant increase of spike amplitude ($p<1*10^{-4}$; **C**). Bars show mean (± the S.E.M.) fluorescent values; ** $p \leq 0.01$.

Figure 6 *Chronic pyruvate treatment reduces basal ROS levels and ROS dependent Zn^{2+}mobilization.*

Panel depicts quantification of basal intracellular ROS levels assessed with the superoxide-sensitive fluorescent indicator HEt. (**A**) HEt loaded 3xTg-AD neurons were evaluated after a 3 day, pyruvate pre-incubation (10 mM; untreated, n=192 neurons, from 7 independent experiments; treated, n=177 neurons from 6 independent experiments). Pyruvate treatment significantly reduced baseline ROS levels in 3xTg-AD neurons (p=0.013). Bars show mean (± the S.E.M.) HEt fluorescence values; $*p \leq 0.05$. Time course of ROS-dependent $[Zn^{2+}]_i$ rises assessed with the Zn^{2+} sensitive dye, FluoZin-3. (**B**) FluoZin-3 loaded 3xTg-AD neurons were evaluated upon a 20 min exposure to the cell oxidant compound, DTDP (25 μM). Blue trace shows mean FluoZin-3 fluorescence values of untreated cultures (n=34 neurons from 6 independent experiments). Red trace shows values of cultures pre-treated for 30 min with pyruvate prior to Zn^{2+} imaging (10 mM ; n=37 neurons from 8 independent experiments). Pyruvate treatment significantly reduced DTDP-driven $[Zn^{2+}]_i$ mobilization (p=0.035; quantified in **C**). Bars show mean (± the S.E.M.) values; $*p \leq 0.05$.

Figure 7 *Pyruvate treatment improves $[Ca^{2+}]_i$ and $[Zn^{2+}]_i$ handling, in 3xTg-AD neurons.*

Time course of NMDA-dependent $[Ca^{2+}]_i$ rises assessed with the low affinity Ca^{2+} indicator Fluo-4FF. (**A**) Fluo-4FF loaded 3xTg-AD neurons were evaluated upon a 10 min exposure to 50 μM NMDA + 15 μM glycine. Blue trace shows mean Fluo-4FF fluorescence values of untreated cultures (n=176 neurons, from 5 independent experiments). Red trace shows mean values of cultures pre-treated for 3 days with 10 mM pyruvate prior to Ca^{2+} imaging (n=271 neurons, from 5 independent experiments). Pyruvate treatment significantly reduced NMDA-driven $[Ca^{2+}]_i$ rises ($p=1*10^{-4}$; quantified in **B**). Bars show mean (± the S.E.M.) values; $**p \leq 0.01$. Time course of NMDA-dependent $[Zn^{2+}]_i$ rises assessed with FluoZin-3. (**C**) FluoZin-3 loaded neurons were evaluated upon a 10 min exposure to 50 μM NMDA + 15 μM glycine. Blue trace shows mean (± the S.E.M.) FluoZin-3 fluorescence values of untreated cultures (n=203 neurons, from 12 independent experiments). Red trace shows FluoZin-3 values of cultures that were pre-treated for 3 days with 10 mM pyruvate prior to Zn^{2+} imaging (n=138 neurons, from 8 independent experiments). Pyruvate treatment significantly reduced NMDA-driven $[Zn^{2+}]_i$ rises ($p=1*10^{-4}$;

quantified in **D**) and promoted full recovery to baseline fluorescence levels. Bars show mean (± the S.E.M.) values; $^{**}p \leq 0.01$.

Figure
Click here to download high resolution image

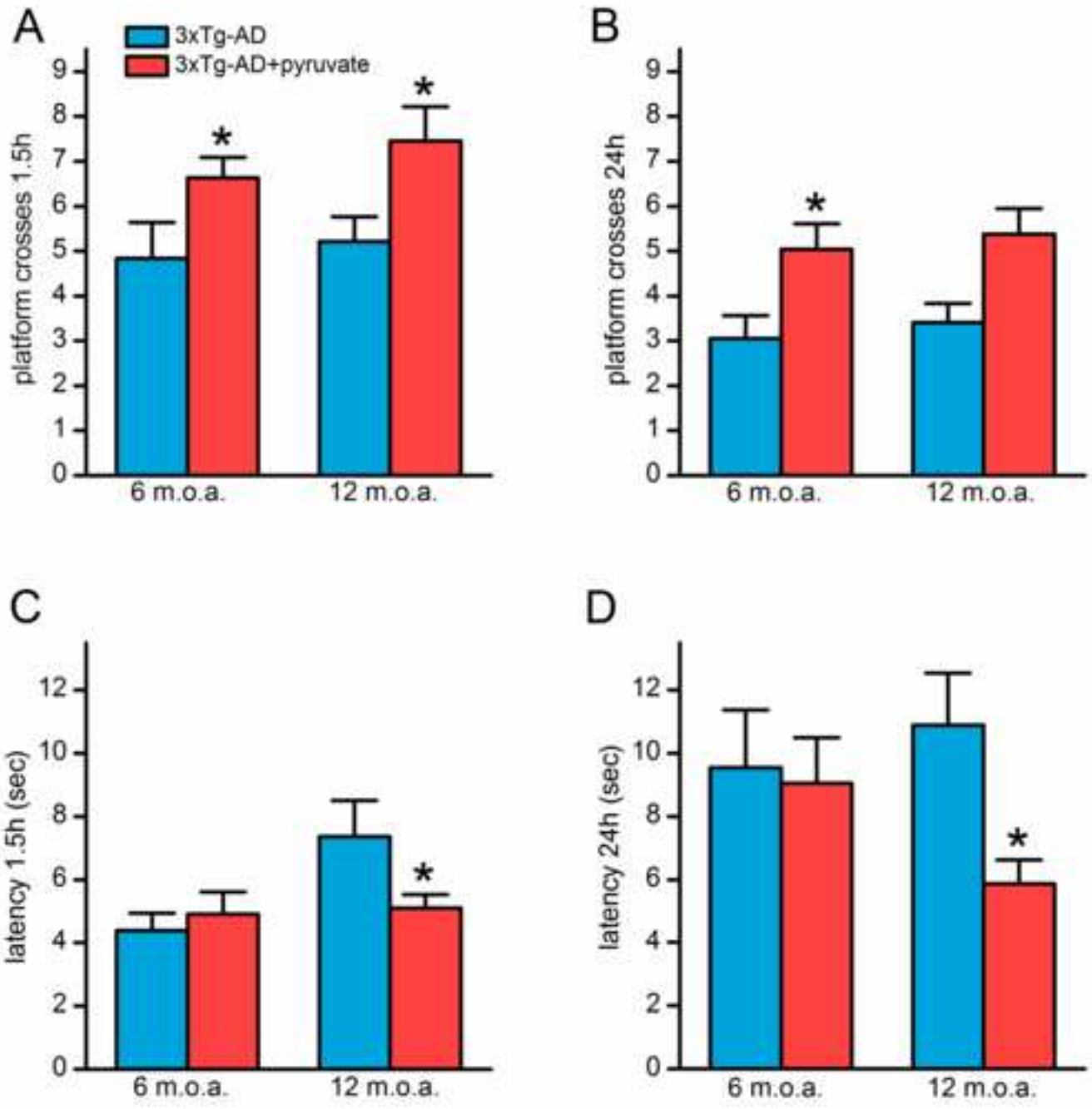

Figure

Click here to download high resolution image

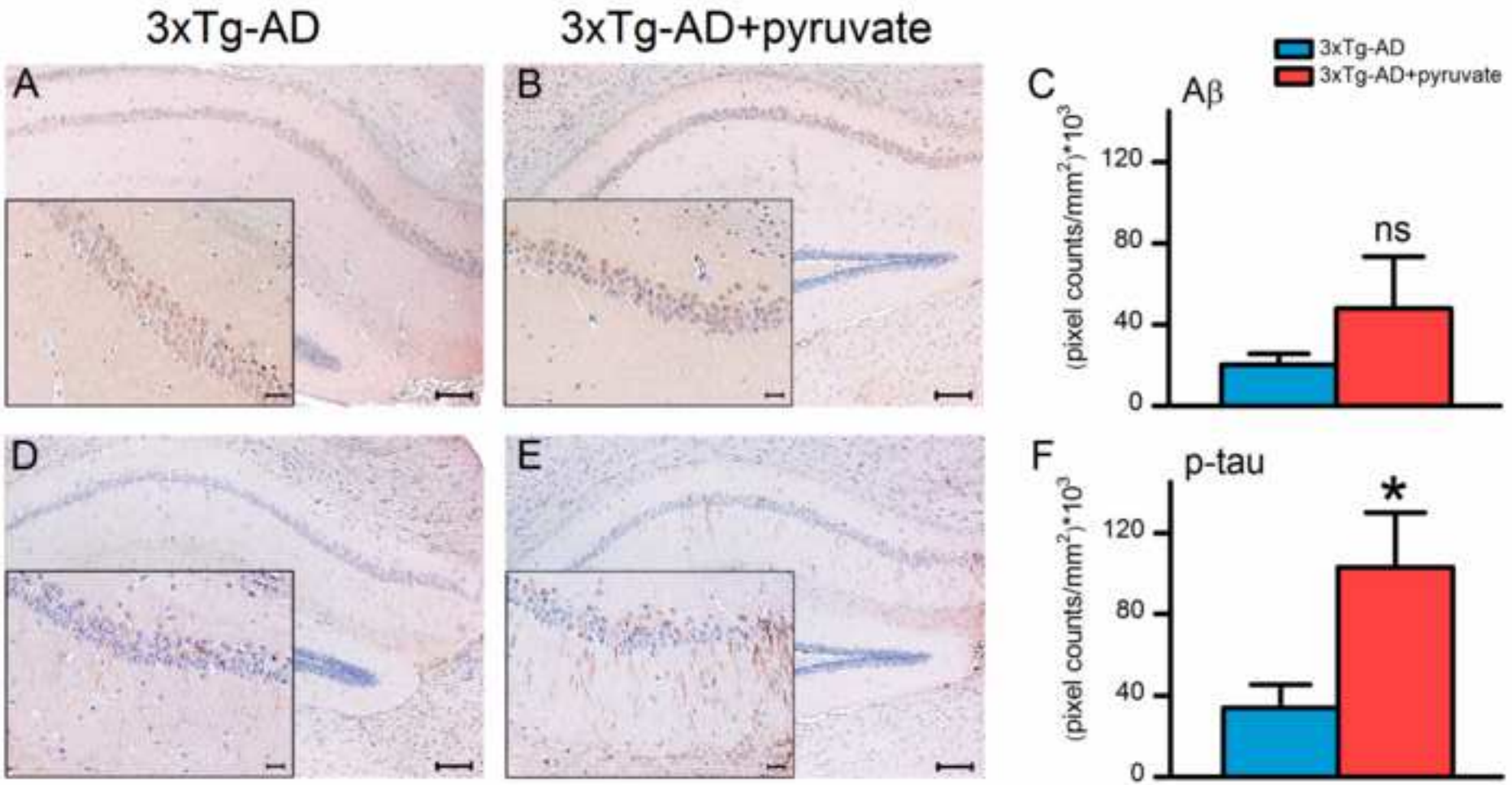

Figure

Click here to download high resolution image

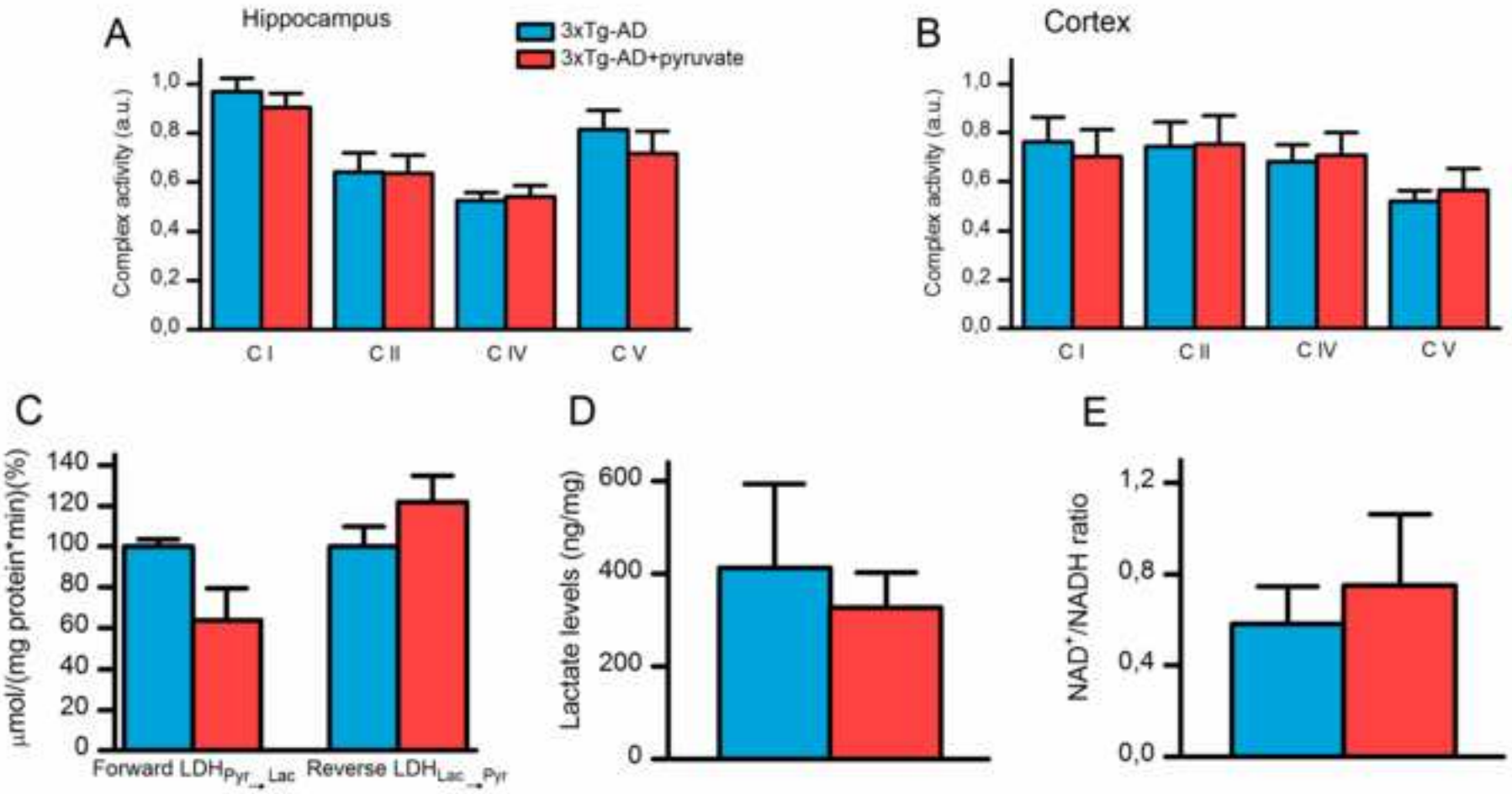

Figure
Click here to download high resolution image

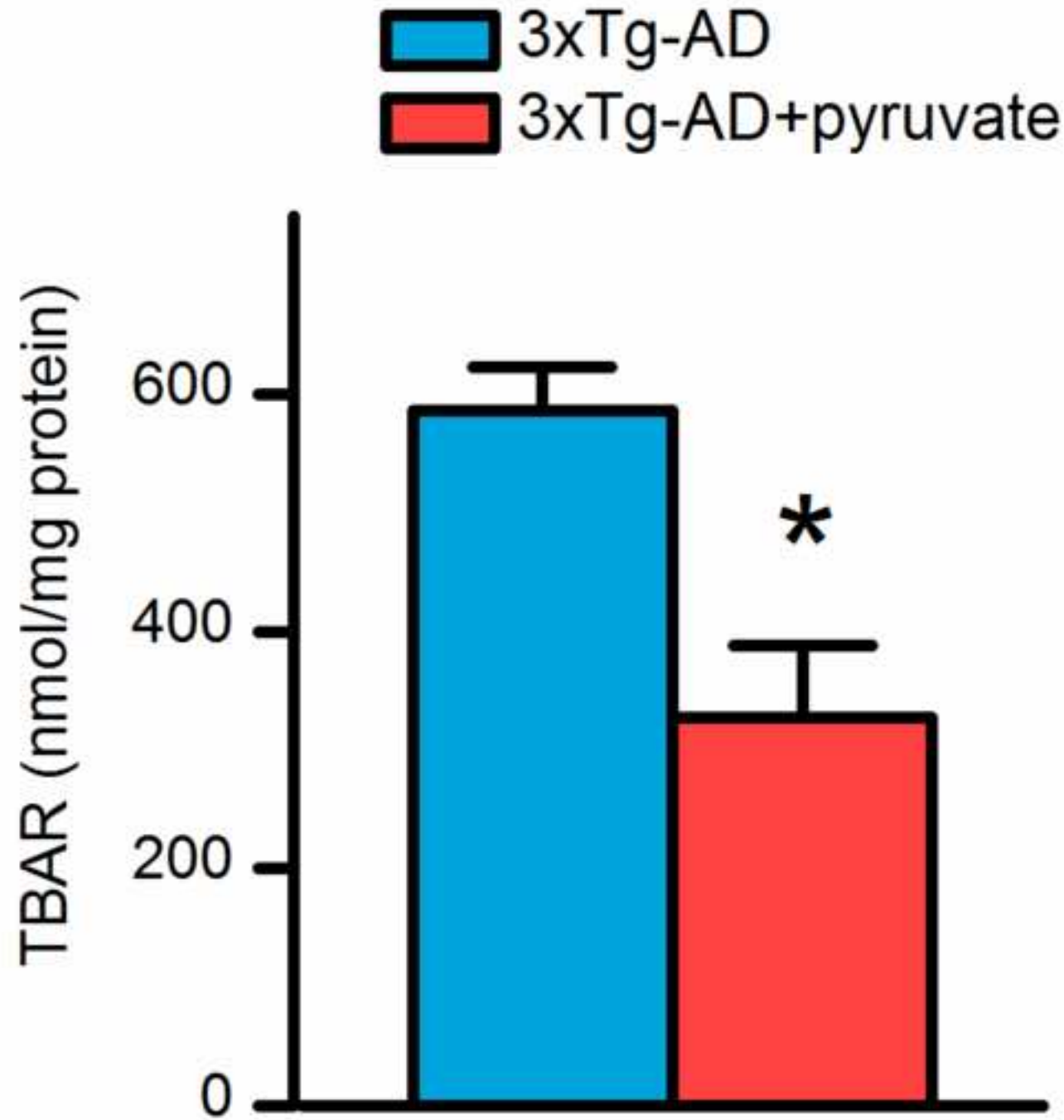

Figure

Click here to download high resolution image

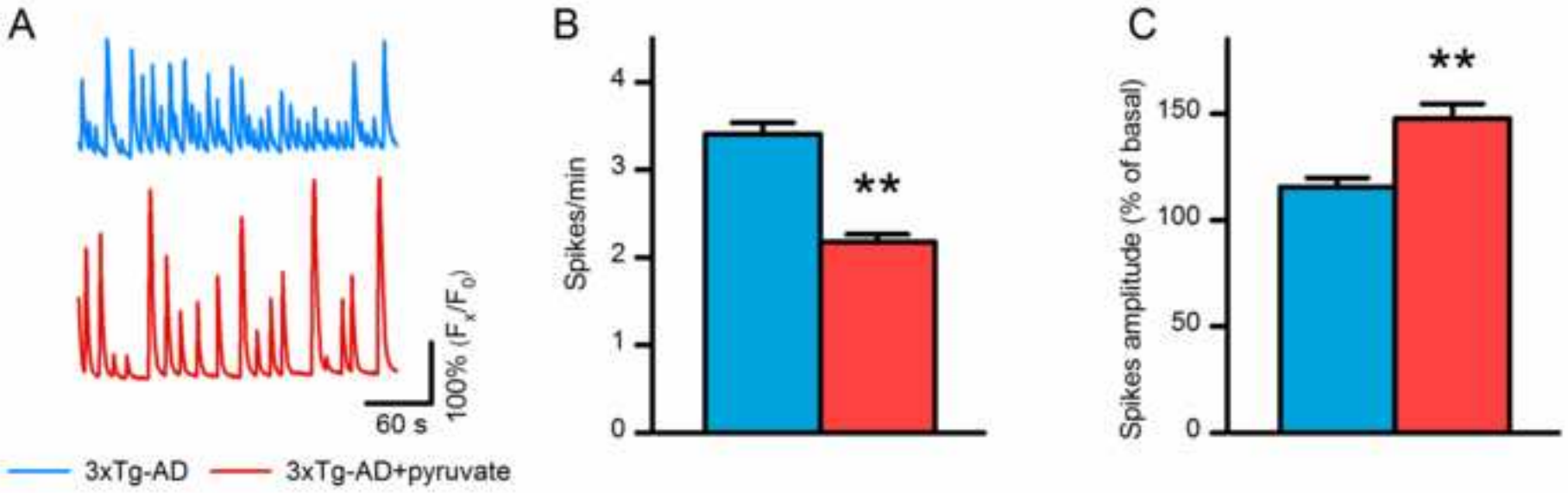

Figure

Click here to download high resolution image

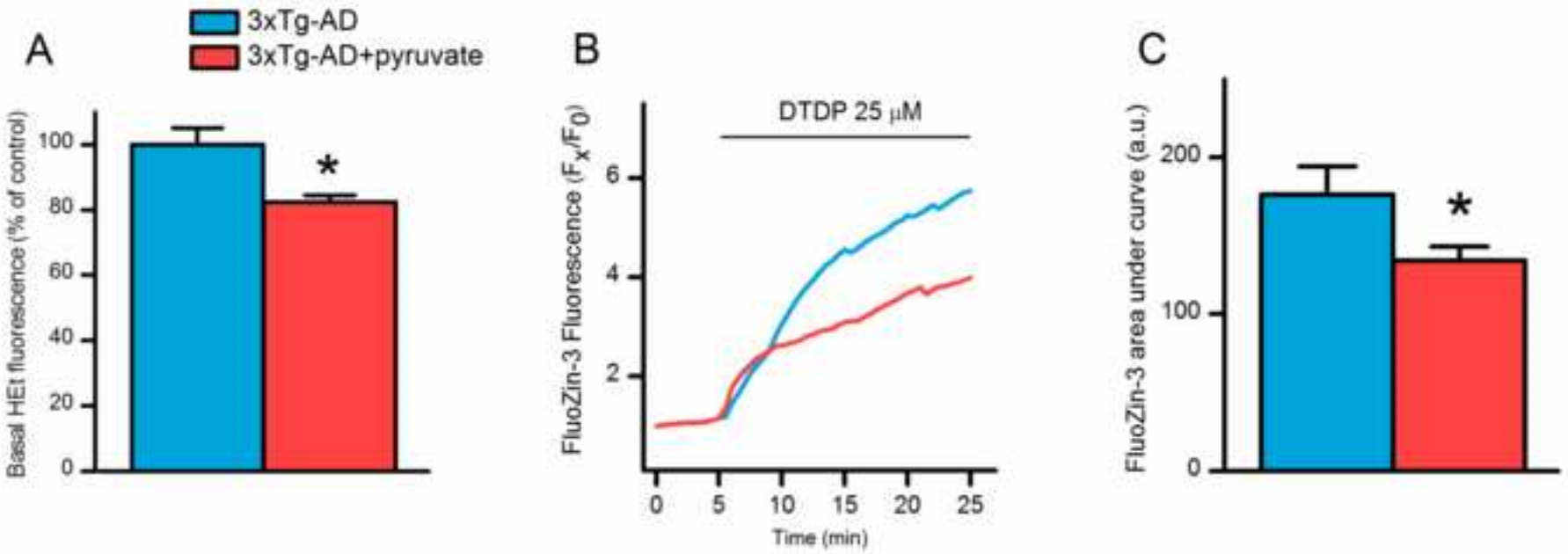

Figure

Click here to download high resolution image